Impact of *d*-band filling on the dislocation properties of bcc transition metals: The case of tantalum-tungsten alloys investigated by density-functional theory

Hong Li,[1,2,3] Claudia Draxl,[1] Stefan Wurster,[3] Reinhard Pippan,[3] and Lorenz Romaner[4,*]

[1]*Institut für Physik and IRIS Adlershof, Humboldt-Universität zu Berlin, Zum Großen Windkanal 6, 12489 Berlin, Germany*

[2]*Paul-Drude-Institut für Festkörperelektronik, Hausvogteiplatz 5-7, 10117 Berlin, Germany*

[3]*Erich Schmid Institute of Materials Science, Austrian Academy of Sciences, Jahn-Straße 12, A-8700 Leoben, Austria*

[4]*Materials Center Leoben Forschung GmbH, Roseggerstraße 18, A-8700 Leoben, Austria*

(Received 6 September 2016; revised manuscript received 18 January 2017; published 15 March 2017)

We address the impact of tantalum alloying on dislocation properties of tungsten. To that aim, we calculate elastic constants, atomic-row displacement energy, dislocation core energy, and Peierls stress for different degrees of alloying within the framework of density-functional theory. We show that the elastic shear constants decrease monotonously with Ta content. Conversely, atomic-row displacement energy and, consequently, core energy and Peierls stress show a nonmonotonous behavior. These quantities peak at 25 at% Ta, indicating a tendency for embrittlement of W at such alloying concentrations. Our findings are in agreement with the experimental literature.

DOI: 10.1103/PhysRevB.95.094114

I. INTRODUCTION

The intrinsic brittleness of the transition metals chromium, molybdenum, and tungsten is a topic of great scientific and technological relevance. Over and above considerable experimental and theoretical activities in the past, the research field is still very active since the phenomenon results from a complex interplay between several factors, including plastic deformation, fracture mode, microstructure, alloying, and impurity elements. In particular, the last point, i.e., the impact of solutes on ductility, is of particular interest from a theoretical point of view and has received considerable attention by the *ab initio* community [1–10]. Although the ductility of a material is a complex phenomenon which can only be completely described by an advanced multiscale simulation approach, several different criteria on the atomic scale have been proposed to reveal trends. This includes the Rice-Thompson (RT) criterion [1], ideal strength [9,10], the Peierls stress [5,7,8] of $\frac{1}{2}\langle 111\rangle$ screw dislocations, and atomic-row displacement energy (ARDE) [2–4]. In these investigations, it is common to differentiate between alloying elements with more valence electrons than W, Mo, and Cr and alloying elements with fewer valence electrons. A quite consistent picture has emerged regarding the former which are found to be ductilizers. This was demonstrated on the basis of the RT criterion [1] and by screw-dislocation modeling [2–5,7,8]. For the elements with smaller valency, the picture is not quite as clear. The RT parameter suggests a weak ductilization [1] in Mo alloys, and a recent work based on ideal shear strength [9] has also proposed a ductilization of Mo upon Nb alloying. In contrast, screw-dislocation simulations suggest an increase of brittleness when alloying Zr into W [8], or Ta into W or Mo [4]. Hence, the overall situation is still controversial and more effort is required to obtain a clear picture for bcc alloying elements.

In this paper, we provide a closer look at the impact of Ta alloying on the Peierls stress of $\frac{1}{2}\langle 111\rangle$ screw dislocations. These screw dislocations are the limiting factor for plastic deformation in bcc metals since they experience high lattice friction [11–13]. This is rooted in their nonplanar core structure. In a previous work [7], we have shown that Ta, unlike Re, does not induce a change from a nondegenerate core to a degenerate core, but rather leaves the core structure unchanged. Hence, the change of the Peierls stress with Ta alloying is decoupled from changes in the core structure. Pure Ta has a considerably smaller Peierls stress than W and is also considerably more ductile. From this, it could be expected that increasing Ta content gradually decreases the Peierls stress. We show here that this is not the case. Rather, a maximum is found at Ta concentrations of about 25 at%. To understand this finding, we first focus on linear elasticity and study the effects of Ta alloying on the elastic constants. Then we address nonlinear elastic effects on the basis of the atomic-row displacement energy, which has been widely used to understand the core structure of screw dislocations. Next, we focus on the core energy and the Peierls stress of the screw dislocations. Finally, we apply a model for the ductile-to-brittle transition (DBT) and show that the changes in Peierls stress at low Ta concentrations lead to a shift of the ductile-to-brittle transition temperature (DBTT) towards higher values. The main attention will be given to W-Ta alloys, but we also include W-Re alloys, which we have focused on previously [5,7]. The comparison between W-Ta and W-Re alloys is interesting because Ta depletes the *d* band, while Re fills it; this directly impacts the quantities under investigation.

II. METHODOLOGY

A. DFT calculations

All density-functional theory (DFT) calculations are performed with QUANTUM ESPRESSO (QE) [14]. A crosscheck with other DFT codes for pure W properties verified the results of QE; see the Appendix. We used norm-conserving pseudopotentials in the Troullier-Martins scheme, generated with FHI98PP. The Perdew-Burke-Ernzerhof (PBE) exchange-correlation functional [15] was used throughout this work. The

*lorenz.romaner@mcl.at

kinetic-energy cutoff for wave functions and charge densities was set to 30 and 120 Ry, respectively. For the Brillouin-zone sampling, we used a 24×24×24 mesh for bulk calculations, a 3×3×17 mesh for atomic-row displacement energy, and a 1×2×16 mesh for the dislocation structures. The dislocation dipole was inserted in a 135-atom supercell (SC), as already outlined elsewhere [5,7].

B. Simulation of alloys

To simulate the W-Me (Me = Ta, Re) alloys, we employ the virtual-crystal approximation (VCA) [16]. Thereby nuclear and electronic charge of W atoms are replaced by effective charges that correspond to a mixture of W and Me atoms according to $Z_x = (1-x)Z_{\mathrm{W}} + xZ_{\mathrm{Me}}$. This way of implementing the VCA is commonly used in all-electron calculations based on augmented plane waves; see, e.g., Refs. [17,18]. We, hence, construct a pseudopotential of an effective atom with intermediate nuclear charge Z_x rather than mixing of pseudopotentials [19,20]. The difference between these methods is most apparent when treating alloying elements that differ strongly in nuclear charge. In the present case, alloying atoms are neighbors in the periodic table, and thus we assume that the different methods would give similar results. In previous investigations of W-Re [5,7], the VCA results for elasticity and the structure of the dislocation core were consistent with supercell calculations. In this work, we perform VCA calculations for W-Me alloys for a series of concentrations. Since Ta is completely soluble in bcc W, a wide range of Ta concentrations of $x = 0.25$, 0.50, and 0.75 is considered, corresponding to 5.75, 5.50, and 5.25 valence electrons, respectively. For Re concentration above $x = 0.25$, the σ phase occurs in the phase diagram; nevertheless, we study values up to $x = 0.50$ to show trends of this dynamically stable bcc lattice [21]. Re concentrations of $x = 0.06, 0.12, 0.25$, and 0.50 correspond to 6.06, 6.12, 6.25, and 6.50 valence electrons, respectively. Together with the pure W and Ta phases, a total of nine different compositions are considered in this study.

C. Elastic constants

To calculate elastic constants, we compute the energy of distorted bcc structures, where the relation between the distorted and original lattice vector is $\mathbf{R}' = \mathbf{R} \bullet (I + \epsilon)$, with I being the identity matrix. Three types of distortions are applied to determine bulk modulus B and shear moduli C' and C_{44}. These are, in Voigt notation, $(\epsilon,\epsilon,\epsilon,0,0,0)$, $(\epsilon,\epsilon,\frac{1}{(1+\epsilon)^2}-1,0,0,0)$, and $(0,0,0,\epsilon,\epsilon,\epsilon)$. Eleven strain ϵ values ranging from −0.05 to +0.05 are considered, where for the respective undistorted structure we apply a very small strain of 0.001 in order to preserve the symmetry for each type of distortion. The calculated total energies are fitted by a polynomial function to determine the second-order elastic constants [22]. A convergence study for pure W is shown in the Appendix.

D. Atomic-row displacements

For the calculation of atomic-row displacement energies, we rely on the methodology outlined previously [4,7]. Thereby a string of atoms is pulled along the [111] direction in a 36-atom unit cell that is characterized by the lattice vectors

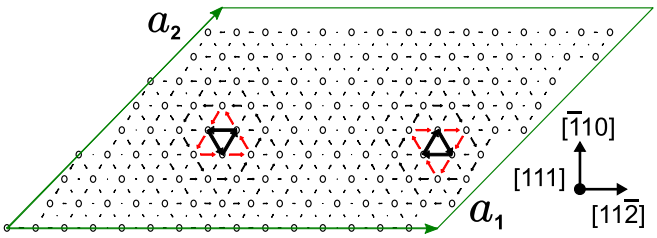

FIG. 1. Dislocation dipole within a (111) plane represented by a differential displacement map [32]. Atoms are indicated by open circles, displacements by arrows. $\boldsymbol{a}_1$ and $\boldsymbol{a}_2$ are unit-cell vectors. Repetition of the unit cell in three dimensions (3D) forms a quadrupolar dislocation arrangement.

$\mathbf{a}_1 = 2\mathbf{u}_{[11\bar{2}]}$, $\mathbf{a}_2 = 3\mathbf{u}_{[\bar{1}10]}$, and $\mathbf{a}_3 = \mathbf{u}_{[111]}$, where $\mathbf{u}_{[11\bar{2}]}$, $\mathbf{u}_{[\bar{1}10]}$, and $\mathbf{u}_{[111]}$ are basis vectors connecting two atoms of the bcc lattice along the specified direction. All atoms are fixed in the z direction while being relaxed within the x-y plane. Such relaxations are important to capture the right trend in core-structure changes [7].

E. Dislocation dipoles

To simulate screw dislocations, we use the periodic dislocation-dipole approach according to which two dislocations with antiparallel burgers vector $\mathbf{b}$ are inserted in a unit cell [5,7,23–29]. The advantage of this method is that periodic boundary conditions are fulfilled and, thus, common electronic-structure codes can be employed. As an infinite solid is modeled, no interaction with surfaces occurs. The core energy has been previously studied in detail for screw dislocations [29–31] and it was found that a quadrupole arrangement converges the core energy faster than hexagonal unit cells, where expansion effects arise. For these reasons, a quadrupole arrangement is also used in this work. More details can be found in the Appendix.

Figure 1 illustrates the geometry of the 135-atom unit cell. Atoms projected on the (111) plane are presented by circles. The distance between two neighboring atoms in the projection plane is $\sqrt{2/3}a_0$, where a_0 is the bulk lattice constant.

III. RESULTS AND DISCUSSION

A. Band filling upon alloying

The impact of Ta and Re alloying on the electronic structure can be monitored via the density of states, which is shown in Fig. 2, going from pure Ta (dark blue) to pure W (gray) and WRe50 (dark red). The bcc pseudogap that appears in pure Ta around 1 eV above the Fermi level is taken as reference energy. Upon alloying, the valence charge increases, shifting the Fermi level to the right. At a Ta content of 25% (WTa25), E_F is located inside the pseudogap, while Re alloying shifts it to even higher energies. This feature is related to the filling of the d band, which is the origin for all alloying-induced modifications of the quantities discussed in the following. Note that the shape of the d band remains basically unchanged upon alloying, suggesting that a rigid-band model [33] would give very similar results as the VCA.

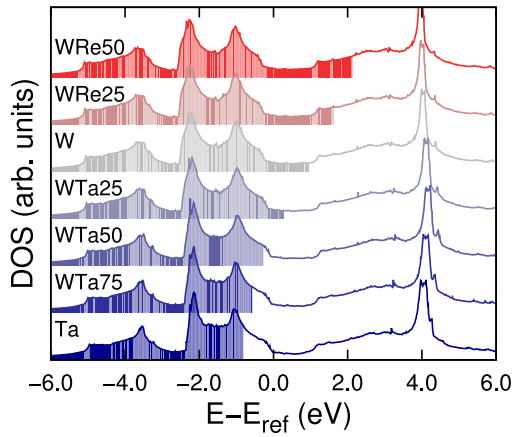

FIG. 2. Band filling of W alloys. The range of occupied states and, hence, the respective Fermi level are indicated by the shaded area. The curves are offset for clarity.

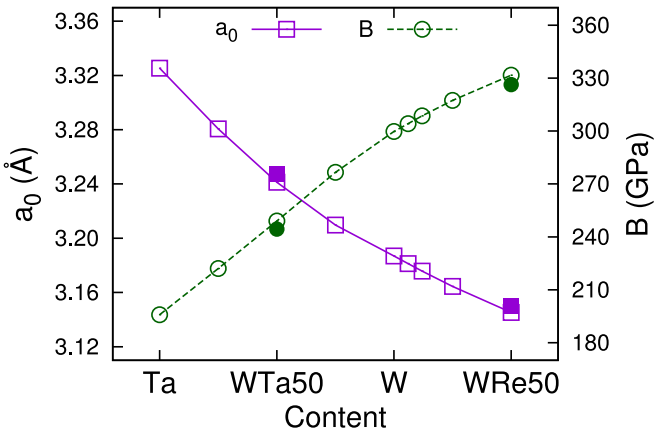

FIG. 3. Lattice constant a_0 and bulk modulus B for W-Me alloys. Open symbols represent VCA calculations for the bcc structure; filled symbols represent SC calculations for the B2 structure.

B. Linear-elastic properties

The band filling has an immediate impact on the linear- and nonlinear-elastic properties. The former will be discussed in this section in terms of elastic constants, while nonlinear effects will emerge from the atomic-row displacement energy shown in the next section.

Table I lists the VCA results together with existing experimental data and results from two supercell (SC) calculations using the B2 structure for 50% Ta and Re content, respectively. Our lattice constants and bulk moduli are in excellent agreement with the experimental and theoretical studies [21,34,35]. We find that C_{44} for pure W and the W-Re alloy is about 12% lower than the experimental values, in agreement with other theoretical studies [8]. We attribute this to shortcomings of semilocal DFT. As illustrated in Fig. 3, the lattice parameter decreases upon d-band filling, while the bulk modulus increases. SC calculations for the B2 structure exhibit small deviations, but show the same general trends as the VCA calculations.

TABLE I. Lattice constant a_0, bulk modulus B, shear moduli C' and C_{44}, and anisotropy $A = C_{44}/C'$ for different compositions.

Method	Alloy	a_0 (Å)	B (GPa)	C' (GPa)	C_{44} (GPa)	A
Expt. [36]	W	3.17	314	163	163	0.99
	WRe10		321	156	171	1.13
	Ta		194	54	87	1.61
VCA	Ta	3.33	196	51	81	1.60
	WTa75	3.28	222	65	79	1.21
	WTa50	3.24	249	95	66	0.69
	WTa25	3.21	277	141	117	0.83
	W	3.19	300	161	143	0.89
	WRe06	3.18	304	158	147	0.93
	WRe12	3.18	309	155	150	0.97
	WRe25	3.16	317	148	158	1.07
	WRe50	3.15	332	126	170	1.34
SC	WTa50	3.25	244	92	76	0.82
	WRe50	3.15	326	106	166	1.57

In Fig. 4, the two shear moduli C_{44} and $C' = (C_{11} - C_{12})/2$ are displayed. It illustrates that C_{44} decreases slowly from pure Ta to WTa50, but increases rapidly thereafter. On the other hand, the tetragonal shear modulus C' first increases continuously from Ta to W, where it exhibits a maximum, but decreases upon alloying with Re. The experimentally observed reduction of C' of W-10%Re in comparison with W [36] is well reproduced by the present calculations.

The elastic anisotropy, $A = C_{44}/C'$, is plotted in Fig. 5. It shows a minimum at 50% Ta concentration (WTa50). The initial band filling leads to an increase in C', but not in C_{44}. At compositions between WTa50 and pure W, C' increases simultaneously with C_{44}. When alloying W with Re, C' starts to decrease, resulting in the V-shaped curve of the anisotropy ratio versus the electronic charge. The minimum elastic anisotropy A occurs at 50% of Ta concentration when C' is much larger than C_{44} (see Fig. 4). Overall, both Ta and Re atoms drastically change the elastic isotropy of W. The alloy becomes more anisotropic with Re alloying and with Ta concentrations higher than 50%, while for Ta concentration lower than 50%, the elastic anisotropy is smaller than that

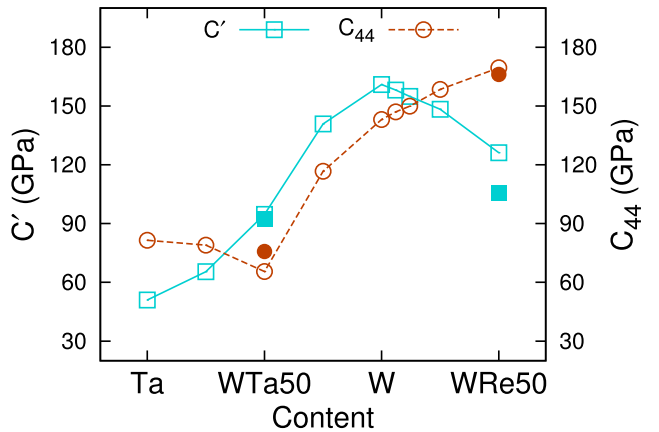

FIG. 4. Shear moduli C' and C_{44} for W-Me alloys based on the VCA (open symbols) and SC (filled symbols) calculations.

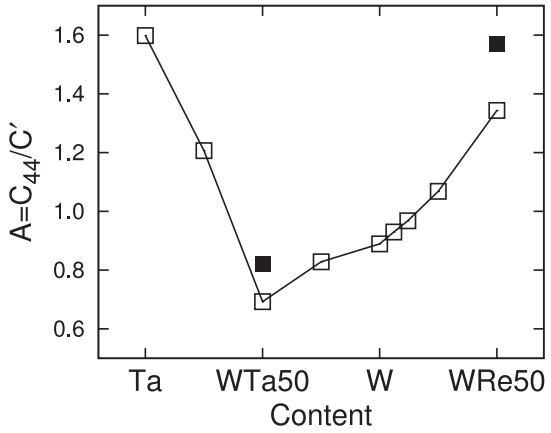

FIG. 5. Elastic anisotropy A for W-Me alloys based on the VCA (open symbols) and SC (filled symbols) calculations.

of pure W. Apparently, only high Ta concentration induces similar changes to A as Re does.

The reduction of both shear moduli with Re and Ta alloying indicates a softening of the lattice in the linear-elastic regime. We note, however, that linear elasticity cannot reliably capture the trends of plasticity, as we will demonstrate in the next section.

C. Atomic-row displacement energy

As investigated previously [3,4,7,37,38], the properties of screw dislocations can be described in more simplified terms by atomic strings along the [111] direction, interacting through so-called atomic-row displacement energy. Such potentials can be parametrized via DFT calculations by simultaneously displacing a row of atoms and computing the corresponding energy cost, which measures the resistance of the lattice with respect to dragging a string of atoms through the crystal. The atomic-row displacement energies E_{ARDE} are shown for all Ta concentrations in Fig. 6. A considerable difference exists between pure Ta and pure W. Pure Ta exhibits much lower values for all displacements h. Remarkably, intermediate Ta concentrations cannot be obtained by interpolation between W and Ta. The WTa25 alloy significantly exceeds the values of W, especially at displacements of $h = 0.3$, while WTa50 reveals a curve almost on top of the one for W. Only at WTa75, the energy has dropped to lower values. We thus conclude that small Ta additions inhibit string displacement, in contrast to what could be expected from the elastic constants, which were found to decrease systematically with the Ta concentration. Note that the ARDE is only linear elastic in the limit of small h, where, e.g., WTa25 reveals smaller energies than W. However, the linear-elastic regime is rather restricted as, at $h = 0.1$, the ARDE of WTa25 is already higher compared to the one of pure W.

An increase of the ARDE upon alloying with elements with less valence electrons has been observed previously for W and Mo [3,4]. Also in Ref. [2], Ta and Hf were found to increase the stiffness against moving a string inside a dislocation core in Mo. In these works, the VCA has not been used, but rather a solute has been put into the string that was then pulled. It is not straightforward to know what alloy this would correspond to in terms of alloying concentration. Our VCA results, on the other hand, are strictly related to an alloying concentration and show that the stiffening occurs between 0 and 50% Ta.

D. Screw-dislocation-line energy, core energy, and Peierls stress

While elastic constants and ARDE are relevant material parameters, direct calculations of dislocations provide an even more definite link to plasticity. We first focus on the energy increase E_{atm} when inserting a dislocation dipole into the unit cell. This energy can be divided into two contributions: one derived from the linear-elastic part, E_{el}, and one from the nonlinear-elastic part of the dislocation core, E_{core},

$$E_{atm} = E_{el} + 2E_{\mathrm{core}}. \quad (1)$$

E_{atm} is obtained from DFT calculations, while E_{el} is calculated from the linear-elastic constants as suggested by Cai *et al.* [24]. For the cutoff radius, we have chosen the burgers vector. E_{atm} and E_{el} do not converge with unit-cell size due to the logarithmic dependence of the dislocation dipole energy on the separation distance [30]. However, the core energy, being a local quantity, converges quickly with unit-cell size, as shown in the Appendix. In Fig. 7, the energy contributions are shown

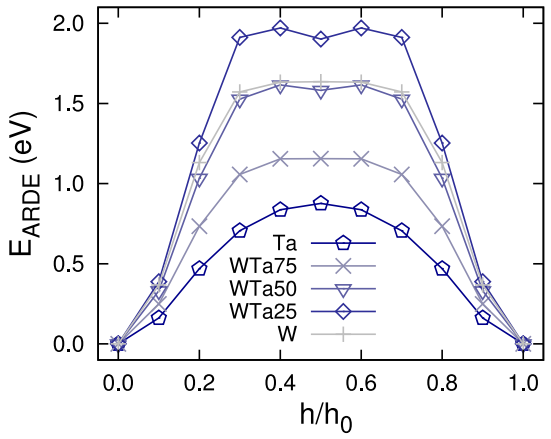

FIG. 6. Atomic-row displacement energy for W-Ta alloys. h is the displacement along the [111] direction.

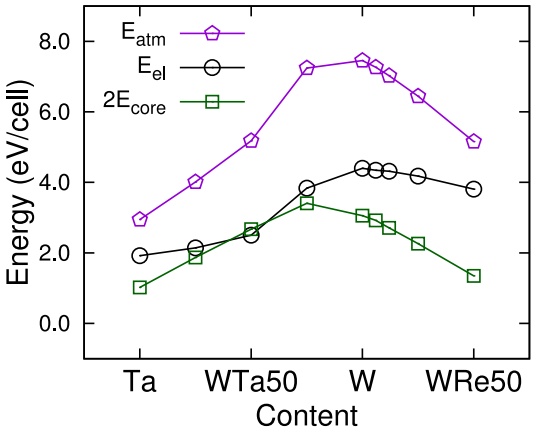

FIG. 7. E_{atm} and its contributions, $2E_{\mathrm{core}}$ and E_{el}, as a function of alloying concentration.

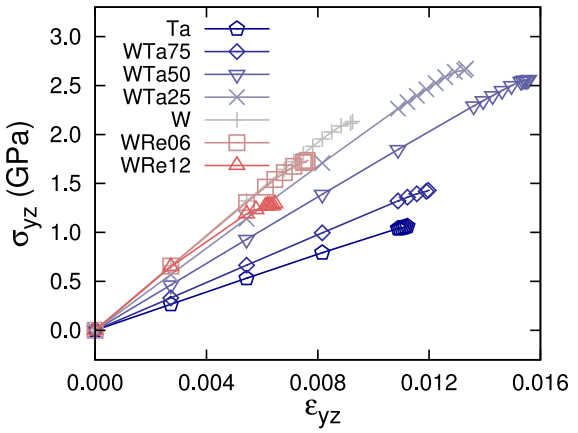

FIG. 8. Stress σ_{yz} vs strain ϵ_{yz} for different W-Ta alloys.

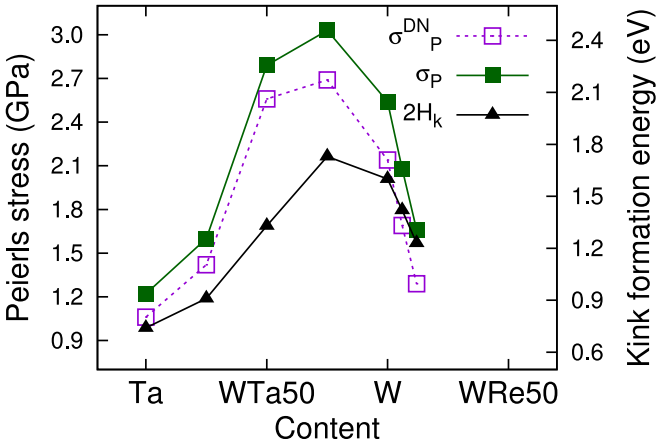

FIG. 9. Peierls stress σ_P^{DN} for dislocation network σ_P for an isolated dislocation, and kink formation energy $2H_k$ for W-Me alloys.

for all alloys. We can see that the elastic part strictly follows the trend investigated earlier and reveals a decay with Ta and Re additions. The core energy, in contrast, reveals an increase with small Ta concentration followed by a decay at higher Ta concentrations. This result is in parallel with the finding obtained in the ARDE, underlining the usefulness of the latter to understand dislocation properties.

To calculate the Peierls stress, we gradually increase the external strain until the dislocations start to move. The strain is applied to the cell vector $\mathbf{a}_2$, so $\mathbf{a}_2' = \mathbf{a}_2 + \epsilon_{yz}\mathbf{u}_{[111]}$, where $\mathbf{u}_{[111]}$ is the basis vector connecting two atoms along the [111] direction in the bcc lattice, and ϵ_{yz} is the external strain that enables the movement of the dislocations. To ensure the accuracy of this calculation, we use a very small step size of 7×10^{-5} in ϵ_{yz}, and relax the atomic structure where the atomic forces are converged within 4.0×10^{-5} Ry/a.u. The corresponding stress-strain diagrams are shown in Fig. 8 for all compositions. The stress-strain curves are basically linear and reveal small deviations only just before the dislocation starts to move. With increasing Ta content, the slope of the stress-strain curves decreases monotonously as expected from linear elasticity. However, the maximum strain reached before the dislocation motion starts varies strongly with the alloying concentration. For the WTa25 and WTa50 alloys, this strain is much higher compared to pure W or pure Ta.

The respective highest stress reached in the curves in Fig. 8 is the Peierls stress of the dislocation network σ_P^{DN}. Note that in the quadrupolar dislocation network, neighboring dislocations attract each other, which slightly lowers the Peierls stress with respect to the isolated dislocation. We correct for these contributions based on a linear-elastic scheme proposed in [5], $\sigma_P = \sigma_P^{DN} - \sigma_P^C$. Details are provided in the Appendix. Values for σ_P^{DN} and σ_P are shown in Fig. 9 and listed in Table II. Clearly, the highest peak in Peierls stress can be recognized for WTa25, which hence exhibits the highest resistance against dislocation motion at 0 K.

E. Impact of Peierls stress changes on the ductile-to-brittle transition

Changes in Peierls stress impact the mobility of $\frac{1}{2}\langle111\rangle$ screw dislocations, which has consequences for the mechanical properties of W-based alloys. For pure W, the connection between Peierls potential, dislocation velocity, and strength has been previously investigated in Ref. [39], while a mechanical model connecting dislocation velocity, toughness, and DBTT has been given in Ref. [40]. In the following, we will elaborate on the connection between our results and this model. The brittle vs ductile response of a material is determined by the competition between crack propagation and dislocation motion at the crack tip. If mobility is low, a crack propagates on its plane by unzipping of atomic bonds and the material is classified as brittle. If dislocation mobility is high, dislocation moving ahead of the crack tip leads to blunting and the materials are classified as ductile. Since dislocation mobility is temperature dependent, the DBT occurs at a critical temperature—the DBTT. The DBTT was calculated for several strain rates by Ref. [40]. For a strain rate of $3.3\times10^{-3}\,\mathrm{s}^{-1}$, DBTT(W) = 523 K. We make use of this result and provide an estimate for the expected shift in DBTT due to Ta alloying in the following. We rely on the well-known velocity relationship [11,39,41]

$$v(T,\sigma) = v_0 \exp\{-H_{kp}(\sigma)/(k_B T)\}, \tag{2}$$

which holds for $\frac{1}{2}\langle111\rangle$ screw dislocations moving by double-kink formation and propagation. In this equation, σ is the effective or thermal component of the resolved shear stress, T is the temperature, and $H_{kp}(\sigma)$ is the stress-dependent double-kink nucleation enthalpy. $H_{kp}(\sigma)$ is chiefly determined by the Peierls potential within which the dislocation moves. In the

TABLE II. Peierls stress σ_P^{DN} for the dislocation network, σ_P for an isolated dislocation, and double-kink formation energy $2H_k$.

Alloy	σ_P^{DN} (GPa)	σ_P (GPa)	$2H_k$ (eV)
Ta	1.06	1.22	0.74
WTa75	1.42	1.60	0.91
WTa50	2.56	2.79	1.33
WTa25	2.69	3.03	1.73
W	2.14	2.54	1.60
WRe06	1.69	2.08	1.42
WRe12	1.29	1.66	1.23

high-temperature and low-stress regime [41],

$$H_{kp}(\sigma) = 2H_k - 2\alpha\sigma, \quad (3)$$

with $2H_k$ being the formation energy of two isolated kinks and α a material parameter. $2H_k$ can be calculated from the Peierls stress as shown in the Appendix. Values are provided in Table II. For pure W, $2H_k = 1.6$ eV, which compares reasonably with the experimental values between 1.75 and 2.06 eV provided in [41]. It is interesting to note that the good agreement does not hold for the Peierls stress which is 2.54 GPa, much higher than the experimental value of about 1 GPa [41]. This overestimation of the Peierls stress at low temperature is a quite general phenomenon which among other explanations has recently been assigned to quantum effects or zero-point motion [42–45].

We can now estimate the DBTT of WTa25 for the strain rate 3.3×10^{-3} s^{-1} by determining the temperature T at which the dislocation velocity in WTa25 becomes equal to the one in W at 523 K. By combining Eqs. (2) and (3), DBTT(WTa25) = DBTT(W)*H_k(WTa25)/H_k(W). Hence, DBTT(WTa25) turns out to be 566 K, i.e., 43 K higher than DBTT(W). This upwards shift only occurs for Ta concentrations of around 25 at% as all other considered concentrations exhibit lower values for H_k. Hence, within the arguments of the model, for all other alloys a ductilization can be expected.

Due to the above arguments, one can expect that strength and tendency for brittle fracture of W alloys is highest around 25% Ta content. Very high Ta additions or small Re additions, on the other hand, should lead to a reduction of strength and increase of ductility. Experimentally, it is well established that W-Re alloys are more ductile compared to pure tungsten, while retaining its good strength [46,47]. Also recent works demonstrate that the alloy W-26wt%Re, which can be regarded to behave identically to the W-25at%Re alloy discussed herein, shows a higher fracture toughness than pure tungsten in the as-worked [48] as well as in the recrystallized state [49]. In contrast, in Ref. [50], it was shown that alloying of 1 at%, 5 at%, and 10 at% Ta into W successively increases the brittleness of the alloy with a transgranular fracture mode. The increasing Ta concentrations investigated in Ref. [50] match with the region where Peierls stress and core energy are found to increase in the calculations. It can, thus, be stated that the simulations properly reproduce the experimental findings for W-25at%Re (higher Re contents are impeded by the σ phase) to moderately alloyed W-Ta. Furthermore, our calculations suggest that only with very high Ta additions, the mechanical properties of W-Ta alloys should improve.

IV. CONCLUSIONS

To summarize, our DFT calculations based on the virtual-crystal approximation reveal the impact of alloying-induced d-band filling on elastic constants, ARDE, core energy, and Peierls stress of $\frac{1}{2}\langle111\rangle$ screw dislocations. We show that linear-elastic shear constants peak for pure W and decrease with adding or removing d electrons by Ta or Re alloying. In contrast, the quantities beyond the linear-elastic regime, i.e., ARDE, core energy, and Peierls stress, exhibit maxima at the d-band occupation of W-Ta alloys with 0–50 at% Ta. Hence, we expect that such Ta additions should impede dislocation motion and lead to embrittlement of W. Only at large Ta contents above 50 at%, an increase in dislocation mobility and ductilization can be expected to occur. Our findings are consistent with experiments [50] available in the literature in contrast to a recent work based on an instability of ideal shear under [100] tension [9]. Due to analogies in d-band filling, the same embrittlement effects are expected to also occur for other solutes which deplete the d band, such as Nb, Hf, Tr, Ti, and V. Furthermore, similar findings are expected when replacing W with Mo as the base material.

All data are available in the NOMAD Repository, DOI http://dx.doi.org/10.17172/NOMAD/2017.02.27-1.

ACKNOWLEDGMENTS

Financial support by the Austrian Federal Government (in particular from Bundesministerium für Verkehr, Innovation und Technologie and Bundesministerium für Wissenschaft, Forschung und Wirtschaft) represented by Österreichische Forschungsförderungsgesellschaft mbH and the Styrian and the Tyrolean Provincial Government, represented by Steirische Wirtschaftsförderungsgesellschaft mbH and Standortagentur Tirol, within the framework of the COMET Funding Programme is gratefully acknowledged.

APPENDIX

1. Convergence of elastic constants

Figure 10 shows the convergence of lattice constant, bulk modulus, and shear moduli of W with respect to the plane-wave energy cutoff and k mesh, respectively. A cutoff of 30 Ry turns out to be sufficient. A $24\times24\times24$ k-point mesh reproduces the elastic constants within 1–2 GPa. Only small deviations of less than 4 GPa are found by using different codes (VASP [51,52], WIEN2k [53]), as shown in Table III. In addition, alternative choices of strain have negligible effects on the elastic constants.

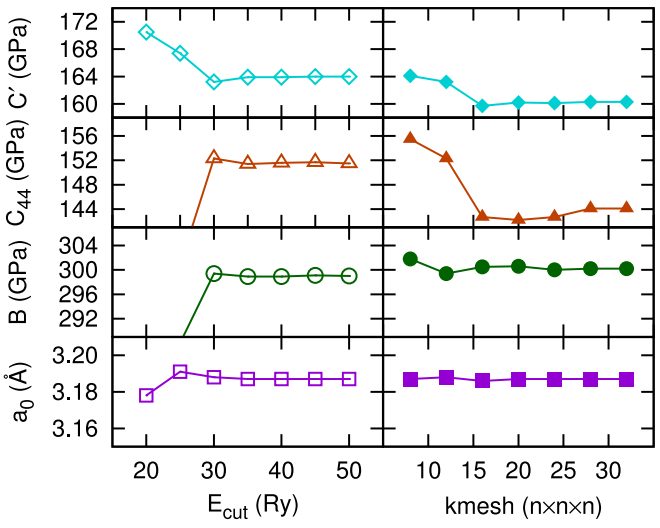

FIG. 10. Convergence of bulk properties as a function of plane-wave cutoff (left) and k mesh (right).

TABLE III. Converged lattice constant a_0, bulk modulus B, shear moduli C' and C_{44}, and anisotropy $A = C_{44}/C'$, for W. RKMAX is the calculation parameter for WIEN2K, which determines the size of the basis set and the accuracy of the calculations.

Code	E_{cut} (Ry)/RKMAX	k mesh	a_0 (Å)	B (GPa)	C' (GPa)	C_{44} (GPa)	A
QE	30.0	24×24×24	3.19	300	161	142	0.89
VASP	29.4	19×19×19	3.19	304	160	141	0.89
WIEN2k	10.0	21×21×21	3.18	300	159	140	0.88

2. Convergence of core energy

In this work, screw dislocations with dislocation lines along [111] directions are treated in a periodic quadrupolar arrangement. The unit cells are characterized by the lattice vectors $\mathbf{a}_1 = r\mathbf{u}_{[11\bar{2}]}$, $\mathbf{a}_2 = 1/2(r\mathbf{u}_{[11\bar{2}]} + s\mathbf{u}_{[\bar{1}10]} + \mathbf{u}_{[111]})$, and $\mathbf{a}_3 = \mathbf{u}_{[111]}$, where $\mathbf{u}_{[11\bar{2}]}$, $\mathbf{u}_{[\bar{1}10]}$, and $\mathbf{u}_{[111]}$ are basis vectors connecting two atoms of the bcc lattice along the specified direction. The parameters r and s have been varied between $r = 3, 5, 7$, and $s = 5, 9, 11$ to explore size effects. The corresponding numbers of atoms in the unit cells are, hence, 45, 135, and 231, respectively. The formation energy E_{atm} and the core energy E_{core} are shown in Fig. 11. For computational convenience, here we used the VASP code. One can see a quick convergence of the core energy, underlining the reliability of the results obtained with 135 atoms.

3. Linear-elastic correction to the Peierls stress

The critical stress at which dislocations move in the periodic arrangement differs somewhat from that of the isolated dislocations since dislocations experience an attractive force whenever the separation between the dislocations is not equal to half the unit-cell vector $\mathbf{a}_1$ (see Fig. 1). This results in an additional stress term, which should be subtracted from the externally applied stress to get the Peierls stress of the isolated dislocation. To make this aspect clear, we show the energy of the dislocation rearrangement as a function of the separation distance between the dislocation in the unit cell, i.e., $E_{atm}(d)$, in Fig. 12. $E_{atm}(d)$ is here calculated from DFT where the atomic positions are fixed to the one expected from linear elasticity and no structural relaxations are carried out to ensure that the dislocations remain separated by d. By Eq. (1), $E_{atm}(d)$ is composed of two contributions: the core term and the linear-elastic term. The core term leads to the periodic oscillation (Peierls potential), while the linear-elastic term leads to the general decay of the energy with distance. This term takes the attraction between neighboring dislocations into account. E_{el} can be obtained separately by anisotropic linear elasticity [30] using the linear-elastic constants from Table I. The result is shown in Fig. 12, where the general good agreement with the DFT result is seen.

When neglecting structural relaxations, the Peierls stress of the dislocation network could be obtained via $\sigma_P^{DN} = \frac{1}{|\mathbf{a}_3|b}\frac{\partial E_{atm}(d)}{\partial d}|_{d=d^*}$, where d^* is the distance for which the derivative is maximal (i.e., $d^* = 7l_n$, with l_n being the period of the Peierls potential). Thereby, $\sigma_P = \frac{2}{|\mathbf{a}_3|b}\frac{\partial E_{\text{core}}(d)}{\partial d}|_{d=d^*}$ would be the Peierls stress of the two isolated dislocations, while $\sigma_P^C = \frac{1}{|\mathbf{a}_3|b}\frac{\partial E_{el}(d)}{\partial d}|_{d=d^*}$ would be the term arising from the attraction of the dislocations. Hence, the Peierls stress of the isolated dislocations is obtained from

$$\sigma_P = \sigma_P^{DN} - \sigma_P^C. \tag{A1}$$

In practice, calculations of the Peierls stress must include relaxations and σ_P^{DN} is rather calculated by applying external strain (see Sec. III D). However, σ_P can be obtained to good approximation via Eq. (A1) since the linear-elastic term will not be strongly affected by the relaxations.

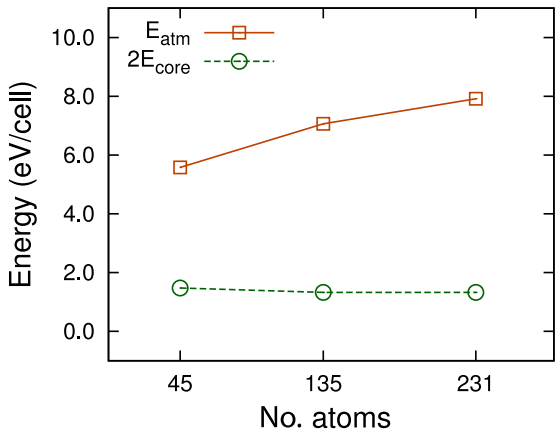

FIG. 11. Dislocation formation energy E_{atm} and core energy E_{core} as a function of number of atoms in the unit cell.

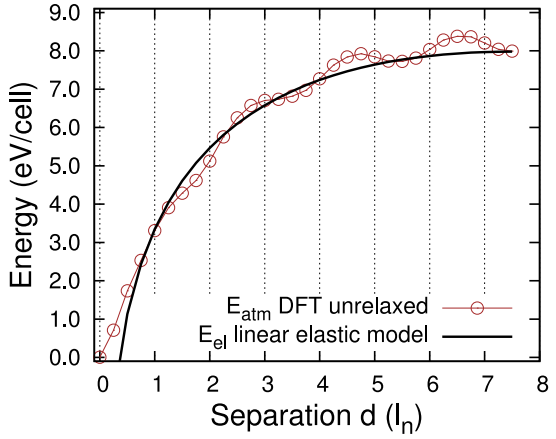

FIG. 12. E_{atm} and E_{el} as a function of separation d. Note that E_{el} is displaced by the average value of $2\overline{E}_{\text{core}}(d) = 3.6$ eV to allow for good comparison with the DFT data.

4. Calculation of kink formation energy

To calculate the kink formation energy from the Peierls stress, we rely on Ref. [41],

$$2H_k = Zl_n\sqrt{2\gamma l_n b\sigma_P}, \tag{A2}$$

with b being the burgers vector, γ the dislocation line tension, and Z a constant depending on the shape of the Peierls potential. In the following, we assume a sinusoidal shape for the Peierls potential, hence $Z = 4/\pi^{3/2}$. According to Ref. [41], the line tension of the isolated dislocation is given by $\gamma = Kb^2/(4\pi)\ln(R/r_c) + E_{\text{core}}$, i.e., the linear-elastic term and the core term. For the linear-elastic term, we rely on the elastic constants in Table I and calculate the energy prefactor K on the basis of linear elasticity [11]. The term $\ln(R/r_c)$ is 4 as proposed in [41]. The so-obtained values for $2H_k$ are shown in Fig. 9 and listed in Table II.

[1] C. B. Geller, R. W. Smith, J. E. Hack, P. Saxe, and E. Wimmer, Scr. Mater. **52**, 205 (2005).
[2] D. R. Trinkle and C. Woodward, Science **310**, 1665 (2005).
[3] N. I. Medvedeva, Y. N. Gornostyrev, and A. J. Freeman, Phys. Rev. B **72**, 134107 (2005).
[4] N. I. Medvedeva, Y. N. Gornostyrev, and A. J. Freeman, Phys. Rev. B **76**, 212104 (2007).
[5] L. Romaner, C. Ambrosch-Draxl, and R. Pippan, Phys. Rev. Lett. **104**, 195503 (2010).
[6] N. G. Kioussis and N. M. Ghoniem, J. Comput. Theor. Nanos. **7**, 1317 (2010).
[7] H. Li, S. Wurster, C. Motz, L. Romaner, C. Ambrosch-Draxl, and R. Pippan, Acta Mater. **60**, 748 (2012).
[8] G. D. Samolyuk, Y. N. Osetsky, and R. E. Stoller, J. Phys.: Condens. Matter **25**, 025403 (2013).
[9] L. Qi and D. C. Chrzan, Phys. Rev. Lett. **112**, 115503 (2014).
[10] J. Pokluda, M. Černý, M. Šob, and Y. Umeno, Prog. Mater. Sci. **73**, 127 (2015).
[11] J. P. Hirth and J. Lothe, *Theory of Dislocations* (McGraw-Hill, New York, 1956).
[12] J. W. Christian, Metallurg. Mater. Trans. A **14**, 1237 (1983).
[13] C. R. Weinberger, G. J. Tucker, and S. M. Foiles, Phys. Rev. B **87**, 054114 (2013).
[14] P. Giannozzi, S. Baroni, N. Bonini, M. Calandra, R. Car, C. Cavazzoni, D. Ceresoli, G. L. Chiarotti, M. Cococcioni, I. Dabo *et al.*, J. Phys.: Condens. Matter **21**, 395502 (2009).
[15] J. P. Perdew, K. Burke, and M. Ernzerhof, Phys. Rev. Lett. **77**, 3865 (1996).
[16] L. Nordheim, Ann. Phys. **401**, 641 (1931).
[17] K.-W. Lee and W. E. Pickett, Phys. Rev. Lett. **93**, 237003 (2004).
[18] C. Neise, S. Schönecker, M. Richter, K. Koepernik, and H. Eschrig, Phys. Status Solidi B **248**, 2398 (2011).
[19] N. J. Ramer and A. M. Rappe, Phys. Rev. B **62**, R743(R) (2000).
[20] L. Bellaiche and D. Vanderbilt, Phys. Rev. B **61**, 7877 (2000).
[21] K. Persson, M. Ekman, and G. Grimvall, Phys. Rev. B **60**, 9999 (1999).
[22] R. Golesorkhtabar, P. Pavone, J. Spitaler, P. Puschnig, and C. Draxl, Comput. Phys. Commun. **184**, 1861 (2013).
[23] S. Ismail-Beigi and T. A. Arias, Phys. Rev. Lett. **84**, 1499 (2000).
[24] W. Cai, V. V. Bulatov, J. Chang, J. Li, and S. Yip, Phys. Rev. Lett. **86**, 5727 (2001).
[25] S. Frederiksen and K. Jacobsen, Philos. Mag. **83**, 365 (2003).
[26] D. E. Segall, A. Strachan, W. A. Goddard, S. Ismail-Beigi, and T. A. Arias, Phys. Rev. B **68**, 014104 (2003).
[27] J. Li, C.-Z. Wang, J.-P. Chang, W. Cai, V. V. Bulatov, K.-M. Ho, and S. Yip, Phys. Rev. B **70**, 104113 (2004).
[28] E. B. Tadmor and R. E. Miller, in *Handbook of Materials Modeling, Part A - Methods*, edited by S. Yip (Springer-Verlag, New York, 2005).
[29] L. Ventelon and F. Willaime, J. Comput.-Aided Mater. **14**, 85 (2007).
[30] W. Cai, V. V. V. Bulatob, J. Chang, J. Li, and S. Yip, Philos. Mag. **83**, 37 (2003).
[31] E. Clouet, L. Ventelon, and F. Willaime, Phys. Rev. Lett. **102**, 055502 (2009).
[32] V. Vítek, R. C. Perrin, and D. K. Bowen, Philos. Mag. **21**, 1049 (1970).
[33] J. Faulkner, Prog. Mater. Sci. **27**, 1 (1982).
[34] C. Jiang, C. Wolverton, J. Sofo, L.-Q. Chen, and Z.-K. Liu, Phys. Rev. B **69**, 214202 (2004).
[35] P. E. A. Turchi, V. Drchal, J. Kudrnovský, C. Colinet, L. Kaufman, and Z.-K. Liu, Phys. Rev. B **71**, 094206 (2005).
[36] R. A. Ayres, G. W. Shannette, and D. F. Stein, J. Appl. Phys. **46**, 1526 (1975).
[37] S. Chiesa, M. Gilbert, S. Dudarev, P. Derlet, and H. V. Swygenhoven, Philos. Mag. **89**, 3235 (2009).
[38] M. R. Gilbert and S. L. Dudarev, Philos. Mag. **90**, 1035 (2010).
[39] R. Gröger and V. Vítek, Acta Mater. **56**, 5426 (2008).
[40] E. Tarleton and S. G. Roberts, Philos. Mag. **89**, 2759 (2009).
[41] D. Brunner, Mater. Trans. **41**, 152 (2000).
[42] R. Gröger and V. Vítek, Philos. Mag. Lett. **87**, 113 (2007).
[43] V. V. Bulatov and W. Cai, Phys. Rev. Lett. **89**, 115501 (2002).
[44] D. Caillard, Acta Mater. **58**, 3493 (2010).
[45] L. Proville, D. Rodney, and M.-C. Marinica, Nat. Mater. **11**, 845 (2012).
[46] G. A. Geach and J. E. Hughes, in *Plansee Proceedings*, edited by F. Benesovsky (Pergamon Press, New York, 1956).
[47] R. I. Jaffee, C. T. Sims, and J. J. Harwood, in *Plansee Proceedings 1958*, edited by F. Benesovsky (Pergamon Press, New York, 1959).
[48] B. Gludovatz, S. Wurster, A. Hoffmann, and R. Pippan, J. Refract. Met. **28**, 674 (2010).
[49] S. Wurster, B. Gludovatz, and R. Pippan, J. Refract. Met. **28**, 692 (2010).
[50] S. Wurster, B. Gludovatz, A. Hoffmann, and R. Pippan, J. Nucl. Mater. **413**, 166 (2011).
[51] G. Kresse and J. Furthmüller, Phys. Rev. B **54**, 11169 (1996).
[52] G. Kresse and D. Joubert, Phys. Rev. B **59**, 1758 (1999).
[53] P. Blaha, K. Schwarz, G. K. H. Madsen, D. Kvasnicka, and J. Luitz, *WIEN2k, An Augmented Plane Wave + Local Orbitals Program for Calculating Crystal Properties* (Karlheinz Schwarz, Techn. Universität Wien, Austria, 2001).